

Article

High-Efficiency Broadband Polarization-Independent Reflective Grating with Double-Layer Dielectric Rectangle Groove in Littrow Mounting

Ge Jin ¹, Wei Jia ¹, Bayanheshig ², Yongfang Xie ¹ and Changhe Zhou ^{1,*}¹ Institute of Photonics Technology, Jinan University, Guangzhou 510632, China² Changchun Institute of Optics, Fine Mechanics and Physics, Chinese Academy of Sciences, Changchun 130033, China

* Correspondence: zhouchanghe@jnu.edu.cn

Abstract: The design and performance of a high-efficiency broadband and polarization-independent reflective grating is reported. The physical mechanism of the gratings can be described by the modal method. By using rigorous coupled wave analysis (RCWA) and simulated annealing (SA) algorithms, the parameters of grating were optimized. The calculated diffraction efficiencies of –1st order for TE and TM polarizations in Littrow mounting exceeded 95%, from 988 nm to 1122 nm, and by over 98% in the bandwidth ranging from 1015 nm to 1085 nm, with the value of polarization-dependent loss (PDL) lower than 0.06 dB. Moreover, the electric field distribution of the grating was simulated by the finite element method (FEM), which demonstrated that most of the energy of the incident light was diffracted to the –1st order and the electric field was distributed almost outside the grating. In addition, the great fabrication tolerances and incident angle tolerance ensured high performance of the designed grating in manufacture and application. With its properties of high efficiency, broadband, and polarization-independence, the designed grating should be of great interest for lots of practical applications, including chirped pulse amplification (CPA), interferometers, and spectrometers.

Keywords: reflective grating; polarization-independent; high efficiency; tolerance analysis



Citation: Jin, G.; Jia, W.; Bayanheshig; Xie, Y.; Zhou, C. High-Efficiency Broadband Polarization-Independent Reflective Grating with Double-Layer Dielectric Rectangle Groove in Littrow Mounting. *Appl. Sci.* **2022**, *12*, 8612. <https://doi.org/10.3390/app12178612>

Academic Editor: Edik U. Rafailov

Received: 7 August 2022

Accepted: 26 August 2022

Published: 28 August 2022

Publisher's Note: MDPI stays neutral with regard to jurisdictional claims in published maps and institutional affiliations.



Copyright: © 2022 by the authors. Licensee MDPI, Basel, Switzerland. This article is an open access article distributed under the terms and conditions of the Creative Commons Attribution (CC BY) license (<https://creativecommons.org/licenses/by/4.0/>).

1. Introduction

As an excellent optical dispersion component, diffraction gratings are widely used in interferometers [1,2], spectrometers [3], spectral beam combining system [4–6], CPA technique [7–9] and so forth. In the mentioned technologies, high-efficiency broadband polarization-independent reflective gratings are more favorable for practical applications. Diffraction efficiency is an important specification for evaluating the quality of diffraction gratings, as it directly affects the output power of the optical system. Furthermore, the broadband and polarization-independent characteristics help to improve the utilization of incident light. Multi-layer dielectric (MLD) gratings attract more attention than conventional reflection metal gratings, because they feature few losses and high diffraction efficiency. Martz et al. designed and manufactured an MLD grating with three etched layers and a measured diffraction efficiency greater than 96% in wavelengths from 780 nm to 820 nm [10]. Mao et al. reported a polarization-independent multi-layer dielectric grating with a diffraction efficiency of over 97%, ranging from 1050 nm to 1080 nm [11]. In Reference [12], a series of polarization-independent multi-layer dielectric gratings were proposed, and the measured diffraction efficiency was over 98%, varying from 1023 nm to 1080 nm. However, the design of MLD gratings requires particular strategies [13–16], which makes the work more complicated. In addition, MLD gratings are often stacked by different materials, causing mechanical stress between the films, which leads to cracks on the grating surface in large-size gratings [17]. This problem can be mitigated by the metallo-dielectric hybrid grating [18]. The solution is to add a metal layer as a mirror to

reduce the number of stacks of films with different refractive indices, thereby reducing the mechanical stress between the films. In addition, metal mirrors can also increase the spectral tolerance and angular tolerance. Federico Canova et al. designed and manufactured a metal–mirror based multi-layer grating and the diffraction efficiency exceeded 97% with 200 nm bandwidth for TE polarization [19]. However, this grating is limited in some practical applications because of the polarization-dependent characteristics. Reference [20] proposed a polarization-independent mixed metal dielectric reflective grating. The -1 st order diffraction efficiencies for TE and TM polarizations were greater than 90% at a bandwidth of more than 120 nm centered at 800 nm. However, the diffraction efficiency of the grating is not satisfactory, which limits the maximum output power of the optical system.

In this paper, a high-efficiency, broadband and polarization-independent double-layer reflective grating with a double-layer dielectric rectangle groove is proposed. The physical mechanisms of the reflective grating can be explained by using the modal method and the parameters of the grating calculated and optimized by the RCWA algorithm [21] and the SA algorithm [22]. In CPA applications, when the short-pulse lasers used Nd: YLF as the gain medium, the center wavelength of the output laser was 1053 nm [23]. Therefore, the operating wavelength of the designed grating was centered at 1053 nm. The diffraction efficiencies of the designed grating, with optimization parameters of -1 st diffraction order for TE and TM polarizations, exceeded 98%, ranging from 1015 nm to 1085 nm, with the Littrow incident angle of 46.35° , and the average diffraction efficiency for the range from 1000 nm to 1100 nm was 98.92%, with an average PDL of 0.051 dB. Simulated by FEM, the electric field distributions of the designed grating for TE and TM polarizations clearly demonstrated the high efficiency of -1 st diffraction order. Moreover, the fabrication tolerances and the dependence of diffraction efficiency on the incident angle are described here in detail. The results clearly demonstrated the feasibility of the designed grating in fabrication and application.

2. Design

The structure of the reflective grating with a double-layer dielectric rectangle groove is shown in Figure 1a. The rectangular groove of the reflective grating consists of two dielectric layers. The first layer of the groove is HfO_2 with the refractive index n_1 and the second layer is made of silicon with the refractive index n_2 . The match layer of the designed grating is made of fused silica with the refractive index n_3 , which serves as the connection layer. When incident light illuminates the grating, the TE-polarized wave (electric field vector perpendicular to the xoz plane) and TM-polarized wave (magnetic field vector perpendicular to the xoz plane) are diffracted to the -1 st diffraction order with high efficiency. Figure 1b shows the refractive indices of the materials of the three-layer dielectric layers at operating wavelength [24–26]. The material of the metal mirror is silver, and its thickness is set to 200 nm, which is significantly larger than the skin depth of the metal to prevent light transmission through the metal mirror to the substrate. Silver has high reflectivity and low absorption at the operating wavelength, which is beneficial to obtain high diffraction efficiency and wide bandwidth of the reflective gratings. However, silver is easily oxidized. The match layer, made of fused silica, is also used as a protective layer. The refractive index of silver at 1053 nm is $0.12483 + 7.3009i$, which was taken from Reference [27]. The period of grating is Λ and the duty cycle of the grating is f , defined as the ratio of ridge width to period. Respectively, h_1 , h_2 and h_3 represent the thickness of the first layer, the second layer and the match layer. The incident angle α is the Littrow angle with incident wavelength of 1053 nm, which can be expressed as:

$$\alpha = \arcsin\left(\frac{\lambda}{2\Lambda}\right) \quad (1)$$

where λ is the wavelength of incident light.

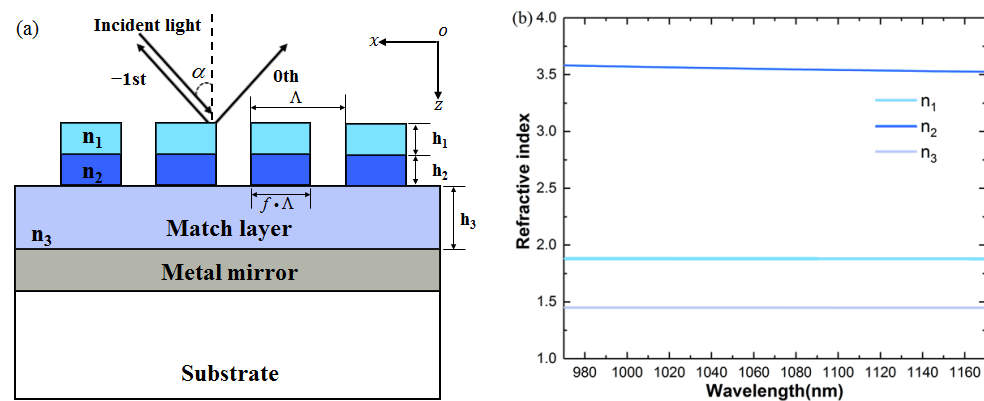


Figure 1. (a) Schematic diagram of the grating and (b) the refractive indices of the material of the dielectric layers.

Diffraction occurs when incident light strikes the grating, and the diffraction order is determined by the grating equation which can be expressed as:

$$\sin \theta_m = \sin \theta_i + m \frac{\lambda}{\Lambda} \tag{2}$$

where θ_i is the incident angle and θ_m is the m th order diffraction angle. (m is an integer.)

When the wavelength and the period satisfy $\frac{\lambda}{2} < \Lambda < \frac{3\lambda}{2}$ only two diffraction orders of $m = 0$ and $m = -1$ are produced. Fewer diffraction orders indicate that the energy of the incident light is more easily coupled to the main diffraction order, which facilitates the design of high-efficiency gratings.

The physical mechanism of the diffraction process of the designed grating can be explained by the modal method [28,29]. Incident light excites propagation modes with different effective refractive indices at each layer. The effective refractive index of the propagation mode is obtained by solving the dispersion equation [30]. The high-density gratings with Littrow incident angle only have two propagation modes corresponding to an effective refractive index greater than 0. The effective refractive index of the other modes is imaginary number and disappears rapidly with propagation. Therefore, these evanescent modes are neglected in the modal method. The two propagation modes produce phase differences as it propagates through each dielectric layer. The propagation modes are coupled to each other at the exit surface of the grating and the efficiency is determined by the accumulated phase difference. Moreover, the diffraction efficiency of the -1 st order reaches its maximum when the accumulated phase difference between the two propagation modes is an odd multiple of $\pi/2$.

In order to obtain a high-efficiency, broadband and polarization-independent grating structure, RCWA was used to calculate the diffraction efficiency of grating. This is also called the Fourier Modal Method. RCWA expands the electromagnetic field and the dielectric constant of the material by a Fourier series, and solves Maxwell’s equations by getting the eigenvalues and eigenvectors of the $n \times n$ matrices, where n is the number of harmonics retained in the field expansion. In RCWA, the truncated order m can control the dimension of the matrices. The relationship between n and m can be expressed as: $n = 2 \times (2m + 1)$. Figure 2 shows the curve of the calculated diffraction efficiency variation with the truncated order. It can be clearly seen that when the truncated order was large enough ($m > 5$), the diffraction efficiency tended to be stable. In this work, the truncated order was set to 20, which was sufficient to ensure the accuracy of the RCWA. Therefore, RCWA is an effective tool for dealing with periodic structures, especially diffraction gratings. In addition, SA algorithms were used to optimize grating parameters $\{f, h_1, h_2, h_3, \Lambda\}$. The

SA algorithms could replace the task of optimizing grating parameters with the task of finding the minimum value of the merit function:

$$MF = \left\{ \frac{1}{N} \sum_{\lambda_i}^{\lambda_N} [(1 - DE_{-1,TE}(\lambda_i))^2 + (1 - DE_{-1,TM}(\lambda_i))^2] \right\}^{1/2} \quad (3)$$

where $DE_{-1,TE}$ and $DE_{-1,TM}$ are the diffraction efficiencies of -1 st order for TE and TM polarizations, respectively.

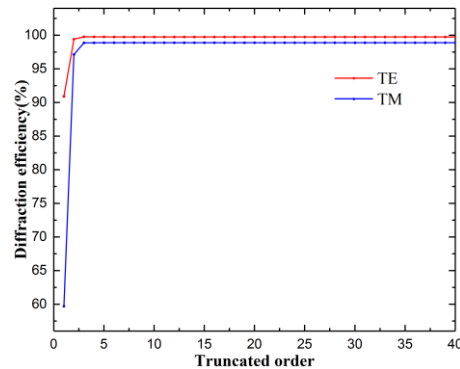


Figure 2. Diffraction efficiencies of -1 st order varied with the truncated order m for TE and TM polarizations at 1053 nm of the designed grating.

In the optimization process, the incident wavelength varied from 1000 nm to 1100 nm with an interval of 5 nm ($N = 21$) and the incident angle was Littrow angle at 1053 nm. Furthermore, the grating parameters were confined in the ranges of: $0.2 < f < 0.8$, $500 \text{ nm} < \Lambda < 1650 \text{ nm}$, $100 \text{ nm} < h_1 < 1000 \text{ nm}$, and $100 \text{ nm} < h_2 < 1000 \text{ nm}$. Finally, the optimized grating had a duty cycle of 0.423, a period of 727.6 nm, a first layer thickness of 256.0 nm, a second layer thickness of 139.2 nm and a match layer of 231.6 nm.

3. Results and Discussion

Figure 3 shows the diffraction efficiency and the PDL of the designed grating with optimized parameters. The diffraction efficiencies of -1 st order for TE and TM polarizations in Littrow incident angle of 46.35° exceeded 95% from 988 nm to 1122 nm, and over 98% in the bandwidth ranging from 1015 nm to 1085 nm. The average diffraction efficiencies for TE and TM polarizations of -1 st order in the range from 1000 nm to 1100 nm was 98.92% and the average diffraction efficiency was defined as:

$$\bar{\eta} = \frac{1}{2} \left\{ \frac{1}{N} \left[\sum_{\lambda_i}^N (DE_{-1,TE}(\lambda_i) + DE_{-1,TM}(\lambda_i)) \right] \right\} \quad (4)$$

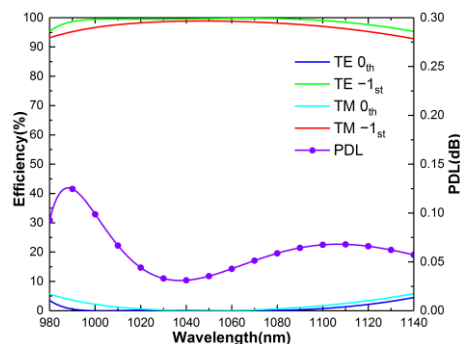


Figure 3. Diffraction efficiencies of -1 st and 0th orders for TE and TM polarizations and the PDL of the designed grating.

As a polarization-independent device, polarization-dependent loss (PDL) was used to evaluate the polarization sensitivity of gratings [31]. The equation of PDL can be expressed as:

$$\text{PDL} = 10 \times \log_{10} \left[\frac{\max(DE_{-1,TE}, DE_{-1,TM})}{\min(DE_{-1,TE}, DE_{-1,TM})} \right] \quad (5)$$

As shown in Figure 3, the value of the PDL of the designed grating was only 0.037 dB at 1053 nm, and the average PDL from 1000 nm to 1100 nm was 0.051 dB which was low enough to ensure the high performance of the polarization-independent characteristic. According to the analysis of the diffraction property, the designed grating achieved excellent and desirable characteristics of high efficiency, broadband and polarization-independence.

In order to verify the operating state of the designed grating with optimized parameters, the electric field distribution of the designed grating was analyzed. Figure 4 shows the electric field distributions for TE and TM polarizations of the designed grating calculated by the FEM [32]. When the plane wave impinged on the grating under Littrow mounting at 1053 nm, the electric field distributions of the incident region and the reflective region were almost the same, which meant that most of the energy of the incident light was diffracted to the -1 st diffraction order. The electric field distribution of the designed grating clearly demonstrated the proof of the high diffraction efficiency of the -1 st order of the designed grating for TE and TM polarizations. In addition, the high laser-induced damage threshold (LIDT) could provide potential for optical system expansion to higher power output [33,34]. It can be seen from Figure 4 that most of the electric field was distributed outside the grating, which helped to increase the LIDT. Moreover, this distribution not only appeared at 1053 nm but also at around the bandwidth from 1000 nm to 1100 nm.

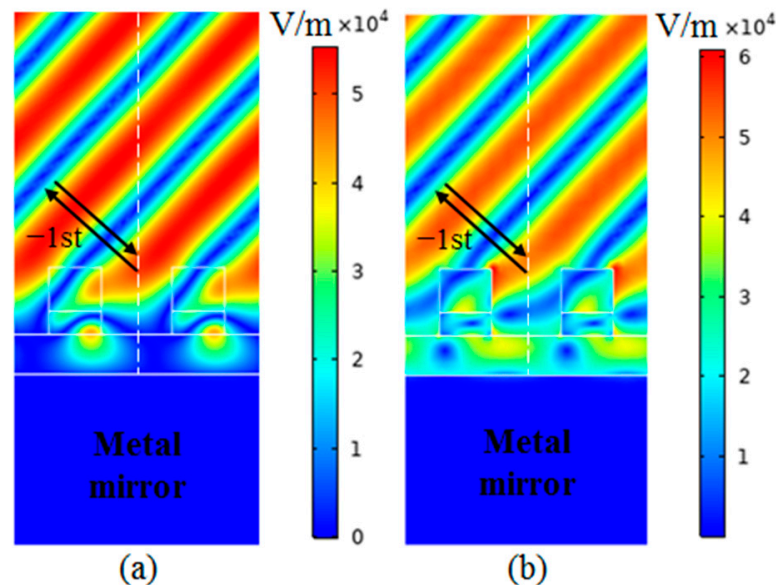


Figure 4. The electric field distributions of the grating at 1053 nm for (a) TE polarization and (b) TM polarization.

In the fabrication process, the structure of the grating always differs from the optimized parameters. Thus, it was necessary to analyze the fabrication tolerance of the designed grating. In addition, the designed grating required a large incidence angle tolerance, because the incidence angle deviates slightly from the intended angle in practical application. In this section, the variation of the diffraction efficiencies with duty cycle and thickness of each layer at Littrow incident angle of 46.35° were calculated by RCWA. There was only one variable of grating parameter in each calculation, the other parameters were fixed as optimized parameters.

Figure 5 shows the diffraction efficiencies of -1 st order versus incident wavelength and duty cycle for both TE and TM polarizations. When the duty cycle ranged from 0.39

to 0.48, the diffraction efficiencies for TE and TM polarizations exceeded 95%, varying from 1000 nm to 1100 nm. The duty cycle is defined as the ratio of ridge width to period, which means that the fabrication tolerance of the line width of the grating was over 65 nm. As shown in Figures 6 and 7, the diffraction efficiencies of -1 st order for TE and TM polarizations exceeded 95%, varying from 1000 nm to 1100 nm, with Littrow incident angle of 46.35° when h_1 ranged from 180 nm to 275 nm and h_2 ranged from 133 nm to 142 nm, respectively. The fabrication tolerance of the second layer was smaller than that of the first layer. According to the previous analysis, since the material of the second layer had a higher refractive index, the corresponding effective refractive index of the second layer was also higher than the first layer. Therefore, the accumulated phase difference between the propagation mode varied significantly with the thickness of the second layer, which led to a smaller fabrication tolerance for the second layer. Moreover, the highly reflective layer consisted of the match layer and the metal mirror. In general, the diffraction efficiency of the metal–mirror based reflective grating exhibits periodic variations with increase of the thickness of the match layer in a wide range [35]. Therefore, the match layer tends to have a certain fabrication tolerance. Figure 8 shows the diffraction efficiencies of -1 st order versus incident wavelength and the thickness of match layer for both TE and TM polarizations. The diffraction efficiencies of -1 st diffraction order for TE and TM polarizations exceeded 95%, varying from 1000 nm to 1100 nm, in Littrow mounting, when h_3 ranged from 220 nm to 247 nm. The properties of great fabrication tolerance of duty cycle and the thickness of the three dielectric layers demonstrated the potential of the designed grating in the fabrication process.

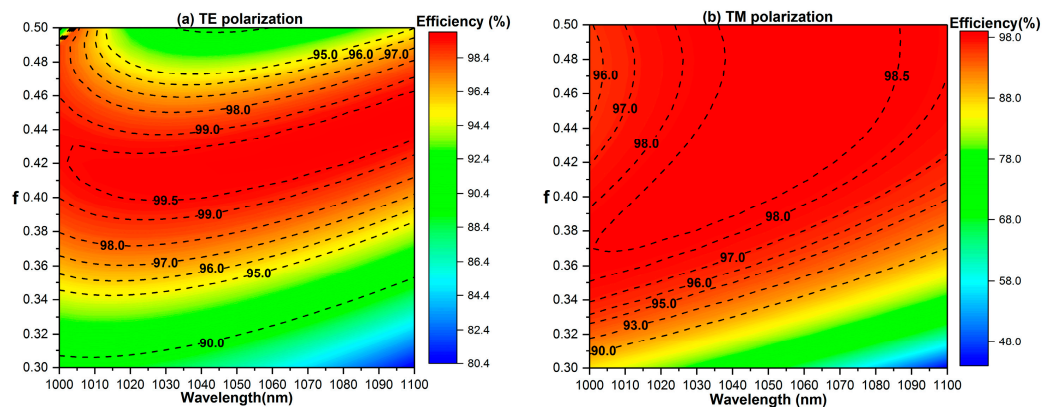


Figure 5. Tolerance analysis of duty cycle. -1 st order diffraction efficiency versus incident wavelength and for (a) TE and (b) TM polarizations.

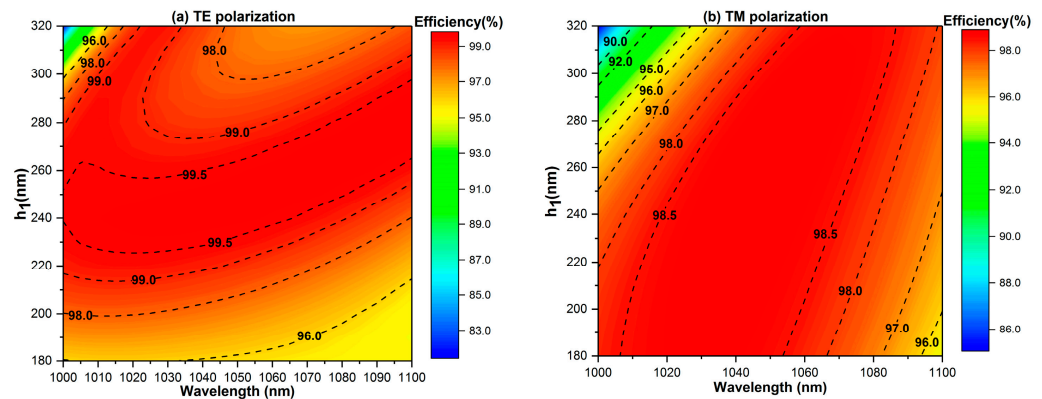


Figure 6. Tolerance analysis of the thickness of HfO_2 layer. -1 st order diffraction efficiency versus incident wavelength and h_1 for (a) TE and (b) TM polarizations.

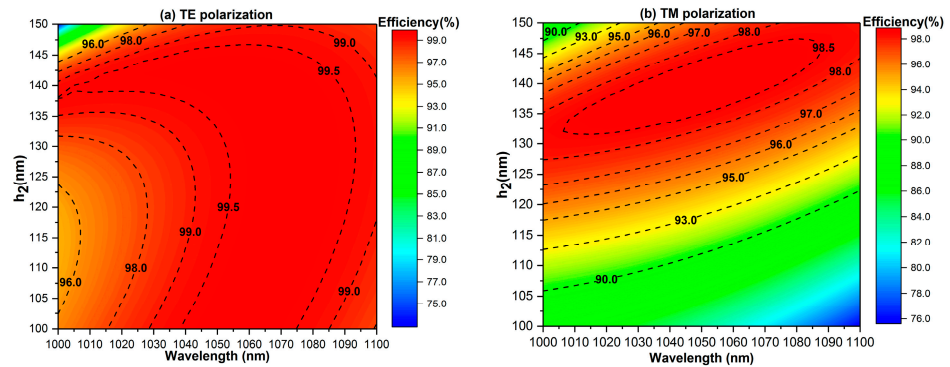


Figure 7. Tolerance analysis of the thickness of silicon layer. –1st order diffraction efficiency versus incident wavelength and h_2 for (a) TE and (b) TM polarizations.

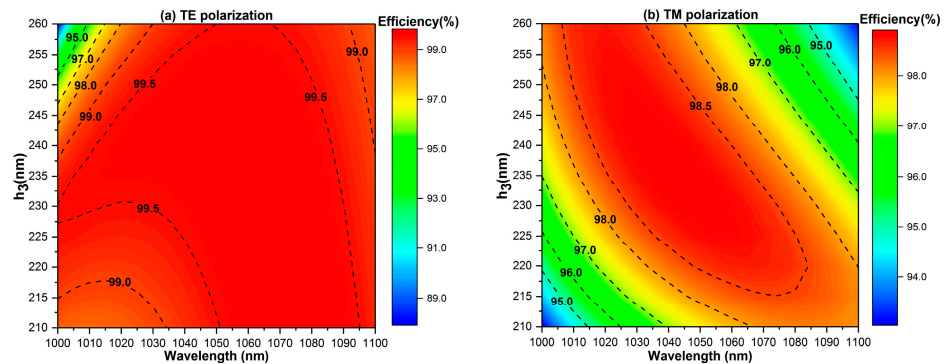


Figure 8. Tolerance analysis of the thickness of match layer. –1st order diffraction efficiency versus incident wavelength and h_3 for (a) TE and (b) TM polarizations.

In addition, the incidence angle of the designed grating was the Littrow angle, so the –1st order diffraction light overlapped with the incident light. In some practical applications, the incidence angle needs to be slightly deviated from the Littrow angle. Therefore, it was necessary to analyze the incident angle tolerance of the designed grating. Figure 9 shows the –1st order diffraction efficiencies versus incident wavelength and incident angle for both TE and TM polarizations. The result showed that the designed grating had a large incidence angle tolerance. Especially in the case of TE polarization, the incident angle had little effect on the diffraction efficiency within ± 10 degrees of the Littrow angle. When the incident angle varied from 39.6° to 54.4° , the diffraction efficiency of –1st order exceeded 90% for TE and TM polarizations, which could meet the requirements of practical application.

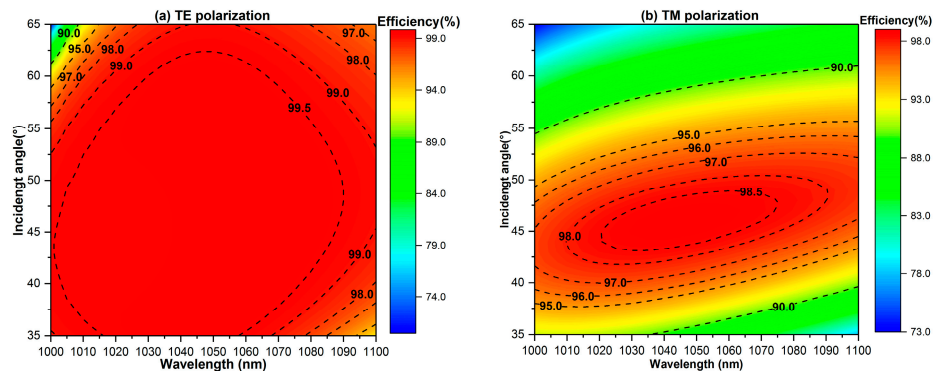


Figure 9. Tolerance analysis of incident angle. –1st order diffraction efficiency versus incident wavelength and incident angle for TE and TM polarizations.

4. Conclusions

The high-efficiency, broadband and polarization-independent characteristics of the designed grating are obtained by the use of proper materials for the dielectric layers and optimization of the parameters of the grating. The grating parameters were optimized by RCWA and SA algorithms and the diffraction process of the reflective grating can be explained by the modal method. The diffraction efficiencies and the PDL of the designed grating with optimized parameters were calculated, and the results showed that the diffraction efficiencies of -1 st order for TE and TM polarizations exceeded 98% ranging, from 1015 nm to 1085 nm, in Littrow mounting (46.35°), and the average efficiency from 1000 nm to 1100 nm reached 98.92% with a low average value of PDL (0.051 dB). Therefore, the designed grating with optimized parameters exhibited better performance than previously reported gratings. The electric field distribution of the designed grating was simulated by FEM and the distribution demonstrated that the designed grating can diffract most of the incident light to the -1 st diffraction order on the operating wavelength and has polarization-independent characteristics. In addition, most of the electric field is distributed outside the grating, which helps to improve the LIDT of the designed grating. Furthermore, the performance of large fabrication tolerance and incident angle tolerance of the designed grating demonstrate proof of the reliability of the grating's fabrication and application. The fabrication of the double-layer dielectric rectangular grating has been reported [36] and the metal mirror can be manufactured by the method of physical vapor deposition [17,37]. In conclusion, the diffraction efficiencies and tolerance analysis of the designed metal-dielectric grating have been expounded in detail. The results indicate the potential of the designed grating in the practical application of interferometers, spectrometers and CPA systems.

Author Contributions: Writing—original draft preparation, G.J.; visualization and supervision, W.J., Bayanheshig, Y.X. and C.Z. All authors have read and agreed to the published version of the manuscript.

Funding: This research was funded by National Natural Science Foundation of China (Grant No. U21A20509), Science and Technology Planning of Guangzhou (Grant No. 202007010001), and Introduced Innovative R&D Team Project under “The Pearl River Talent Recruitment Program” (Grant No. 2019ZT08Z779).

Institutional Review Board Statement: No applicable.

Informed Consent Statement: No applicable.

Data Availability Statement: The data used to support the findings of this study are available from the authors upon request.

Conflicts of Interest: The authors declare no conflict of interest.

References

1. Qi, J.; Wang, Z.; Huang, J.; Wang, Q.; Gao, J. Heterodyne interferometer with two parallel-polarized input beams for high-resolution roll angle measurement. *Opt. Express* **2019**, *27*, 13820–13830. [[CrossRef](#)]
2. Wang, B.; Wang, X.; Li, Z.; Sasaki, O. Sinusoidal phase-modulating laser diode interferometer insensitive to intensity modulation for real-time displacement measurement with feedback control system. *Opt. Commun.* **2012**, *285*, 3827–3831. [[CrossRef](#)]
3. Brand, M.; Zhang, B.; Onural, D.; Al Qubaisi, K.; Popović, M.; Dostart, N.; Wagner, K. High-resolution and compact serpentine integrated grating spectrometer. *JOSA B* **2021**, *38*, A75–A85. [[CrossRef](#)]
4. Wirth, C.; Schmidt, O.; Tsybin, I.; Schreiber, T.; Eberhardt, R.; Limpert, J.; Andreas, T.; Klaus, L.; Michael, G.; Eric ten, H.; et al. High average power spectral beam combining of four fiber amplifiers to 8.2 kW. *Opt. Lett.* **2011**, *36*, 3118–3120. [[CrossRef](#)] [[PubMed](#)]
5. Zheng, Y.; Yang, Y.; Wang, J.; Hu, M.; Liu, G.; Zhao, X.; Chen, X.; Liu, K.; Zhao, C.; He, B.; et al. 10.8 kW spectral beam combination of eight all-fiber superfluorescent sources and their dispersion compensation. *Opt. Express* **2016**, *24*, 12063–12071. [[CrossRef](#)] [[PubMed](#)]
6. Yu, C.X.; Augst, S.J.; Redmond, S.M.; Goldizen, K.C.; Murphy, D.V.; Sanchez, A.; Fan, T.Y. Coherent combining of a 4 kW, eight-element fiber amplifier array. *Opt. Lett.* **2011**, *36*, 2686–2688. [[CrossRef](#)]
7. Strickland, D.; Mourou, G. Compression of amplified chirped optical pulses. *Opt. Commun.* **1985**, *55*, 447–449. [[CrossRef](#)]

8. Blanchot, N.; Bar, E.; Behar, G.; Bellet, C.; Bigourd, D.; Boubault, F.; Boubault, C.; Chappuis, H.; Coïc, C.; Damiens-Dupont, O.; et al. Ruyter Experimental demonstration of a synthetic aperture compression scheme for multi-Petawatt high-energy lasers. *Opt. Express* **2010**, *18*, 10088–10097. [[CrossRef](#)]
9. Habara, H.; Xu, G.; Jitsuno, T.; Kodama, R.; Suzuki, K.; Sawai, K.; Kondo, K.; Miyanaga, N.; Tanaka, K.A.; Mima, K.; et al. Pulse compression and beam focusing with segmented diffraction gratings in a high-power chirped-pulse amplification glass laser system. *Opt. Lett.* **2010**, *35*, 1783–1785. [[CrossRef](#)]
10. Martz, D.H.; Nguyen, H.T.; Patel, D.; Britten, J.A.; Alessi, D.; Krous, E.; Wang, Y.; Larotonda, M.A.; George, J.; Knollenberg, B.; et al. Large area high efficiency broad bandwidth 800 nm dielectric gratings for high energy laser pulse compression. *Opt. Express* **2009**, *17*, 23809–23816. [[CrossRef](#)]
11. Mao, X.; Li, C.; Qiu, K.; Zeng, L.; Li, L.; Chen, X.; Wu, J.; Liu, Z.; Fu, S.; Hong, Y. Design and fabrication of 1300-line/mm polarization-independent reflection gratings for spectral beam combining. *Opt. Commun.* **2020**, *458*, 124883. [[CrossRef](#)]
12. Chen, J.; Zhang, Y.; Wang, Y.; Kong, F.; Huang, H.; Wang, Y.; Jin, Y.; Chen, P.; Xu, J.; Shao, J. Polarization-independent broadband beam combining grating with over 98% measured diffraction efficiency from 1023 to 1080 nm. *Opt. Lett.* **2017**, *42*, 4016–4019. [[CrossRef](#)] [[PubMed](#)]
13. Svakhin, A.S.; Sychugov, V.A.; Tikhomirov, A.E.; Mason, A. Efficient diffraction elements for TE-polarized waves. *Soviet Phys. Tech. Phys.* **1991**, *36*, 1038–1040.
14. Svakhin, A.S.; Sychugov, V.A.; Tikhomirov, A.E. Diffraction gratings with high optical strength for laser resonators. *Quantum Electron.* **1994**, *24*, 233. [[CrossRef](#)]
15. Yin, Z.; Yu, J.; Lu, Y.; Zhou, C. Broadband high-efficiency gratings operating at the 2nd order designed by simplified modal method. *IEEE Photon. Technol. Lett.* **2020**, *32*, 309–312. [[CrossRef](#)]
16. Bonod, N.; Neauport, J. Diffraction gratings: From principles to applications in high-intensity lasers. *Adv. Opt. Photon.* **2016**, *8*, 156–199. [[CrossRef](#)]
17. Palmier, S.; Neauport, J.; Baclet, N.; Lavastre, E.; Dupuy, G. High reflection mirrors for pulse compression gratings. *Opt. Express* **2009**, *17*, 20430–20439. [[CrossRef](#)]
18. Bonod, N.; Neauport, J. Optical performance and laser induced damage threshold improvement of diffraction gratings used as compressors in ultra-high intensity lasers. *Opt. Commun.* **2006**, *260*, 649–655. [[CrossRef](#)]
19. Canova, F.; Uteza, O.; Chambaret, J.P.; Flury, M.; Tonchev, S.; Fechner, R.; Parriaux, O. High-efficiency, broad band, high-damage threshold high-index gratings for femtosecond pulse compression. *Opt. Express* **2007**, *15*, 15324–15334. [[CrossRef](#)]
20. Hu, A.; Zhou, C.; Cao, H.; Wu, J.; Yu, J.; Jia, W. Polarization-independent wideband mixed metal dielectric reflective gratings. *Appl. Opt.* **2012**, *51*, 4902–4906. [[CrossRef](#)]
21. Moharam, M.G.; Gaylord, T.K. Rigorous coupled-wave analysis of planar-grating diffraction. *J. Opt. Soc. Am.* **1981**, *71*, 811–818. [[CrossRef](#)]
22. Kirkpatrick, S.; Gelatt, C.D.; Vecchi, M.P. Optimization by simulated annealing. *Science* **1983**, *220*, 671–680. [[CrossRef](#)] [[PubMed](#)]
23. Frei, B.; Balmer, J.E. 1053-nm-wavelength selection in a diode-laser-pumped Nd: YLF laser. *Appl. Opt.* **1994**, *33*, 6942–6946. [[CrossRef](#)] [[PubMed](#)]
24. Al-Kuhaili, M.F. Optical properties of hafnium oxide thin films and their application in energy-efficient windows. *Opt. Mater.* **2004**, *27*, 383–387. [[CrossRef](#)]
25. Green, M.A. Self-consistent optical parameters of intrinsic silicon at 300 K including temperature coefficients. *Sol. Energ. Mat. Sol. Cells* **2008**, *92*, 1305–1310. [[CrossRef](#)]
26. Malitson, I.H. Interspecimen comparison of the refractive index of fused silica. *J. Opt. Soc. Am.* **1965**, *55*, 1205–1209. [[CrossRef](#)]
27. Yang, H.U.; D'Archangel, J.; Sundheimer, M.L.; Tucker, E.; Boreman, G.D.; Raschke, M.B. Optical dielectric function of silver. *Phys. Rev. B* **2015**, *91*, 235137. [[CrossRef](#)]
28. Xie, Y.; Jia, W.; Sun, P.; Xiang, C.; Jin, G.; Liu, W.; Zhou, B.; Zhou, C. Ultra-broadband polarization-independent high-efficiency transmission grating based on three-layer dielectric rectangle groove. *J. Opt.* **2021**, *23*, 075606. [[CrossRef](#)]
29. Hu, A.; Zhou, C.; Cao, H.; Wu, J.; Yu, J.; Jia, W. Modal analysis of high-efficiency wideband reflective gratings. *J. Opt.* **2012**, *14*, 055705. [[CrossRef](#)]
30. Botten, I.C.; Craig, M.S.; McPhedran, R.C.; Adams, J.L.; Andrewartha, J. The dielectric lamellar diffraction grating. *Opt. Acta.* **1981**, *28*, 413–428. [[CrossRef](#)]
31. Lichtman, E. Limitations imposed by polarization-dependent gain and loss on all-optical ultralong communication systems. *J. Lightwave Technol.* **1995**, *13*, 906–913. [[CrossRef](#)]
32. Delort, T.; Maystre, D. Finite-element method for gratings. *J. Opt. Soc. Am. A* **1993**, *10*, 2592–2601. [[CrossRef](#)]
33. Hocquet, S.; Neauport, J.; Bonod, N. The role of electric field polarization of the incident laser beam in the short pulse damage mechanism of pulse compression gratings. *Appl. Phys. Lett.* **2011**, *99*, 061101. [[CrossRef](#)]
34. Stuart, B.C.; Feit, M.D.; Herman, S.; Rubenchik, A.M.; Shore, B.W.; Perry, M.D. Optical ablation by high-power short-pulse lasers. *J. Opt. Soc. Am. B* **1996**, *13*, 459–468. [[CrossRef](#)]
35. Zheng, J.; Zhou, C.; Feng, J.; Cao, H.; Lu, P. A metal-mirror-based reflecting polarizing beam splitter. *J. Opt. A-Pure Appl. Opt.* **2008**, *11*, 015710. [[CrossRef](#)]

-
36. Shiozaki, M.; Shigehara, M. Novel design of polarization independent multi-layer diffraction grating with high angular dispersion. *SEI Technol. Rev.* **2005**, *59*, 27–31.
 37. Neauport, J.; Bonod, N.; Hocquet, S.; Palmier, S.; Dupuy, G. Mixed metal dielectric gratings for pulse compression. *Opt. Express* **2010**, *18*, 23776–23783. [[CrossRef](#)]